Investigation of complex ionization amplitudes in cadmium by (e,2e) spectroscopy

N. L. S. Martin, D. B. Thompson, R. P. Bauman, and M. Wilson*

Department of Physics and Astronomy, University of Kentucky, Lexington, Kentucky 40506-0055

(Received 22 June 1994)

High-resolution $(e,2e)$ energy spectra are presented which enable the isolation of interference effects between $J=0,1,2$ multipoles in electron-impact ionization of cadmium. It is found that both resonant and nonresonant processes are important. Relative magnitudes and phases of ionization amplitudes are obtained which disagree with plane-wave Born approximation calculations.

PACS number(s): 34.80.Dp, 32.80.Dz, 35.10.−d

I. INTRODUCTION

An electron-electron coincidence, or $(e,2e)$, experiment investigates processes in which an incident electron of energy E_0 ionizes a neutral atom or molecule X, producing a singly charged ion X^+ in the ground or an excited state. Ionization is the result of either the direct excitation of a bound atomic electron into the continuum, or a resonant process via an intermediate autoionizing state X^{**} coupled to the continuum. The two outgoing electrons (1 and 2) are detected in (delayed) coincidence at predetermined angles and energies, subject to the energy balance $E_0=E_1+E_2+E_{IP}$, where E_{IP} is the threshold energy or ionization potential (IP) of the chosen final ion state.

$(e,2e)$ experiments fall into different categories depending on the kinematics [1]. Here we are concerned with coplanar asymmetric geometry (all electrons in the same plane) where one of the outgoing electrons is fast and the other is slow; they may then be labeled "scattered" and "ejected" electrons, respectively. We shall use a coordinate system where in-plane angles are measured with respect to the incident electron direction. A typical experiment holds E_{sc}, θ_{sc}, and $E=E_{ej}$ fixed, while θ_{ej} is varied. Experiments on direct ionization find strong angular correlations between scattered and ejected electrons: $(e,2e)$ ejected-electron angular distributions show two pronounced features, the forward, or binary $(+\mathbf{K})$ peak, and the backward, or recoil $(-\mathbf{K})$ peak, where $\mathbf{K}$ is the momentum transferred in the collision [2]. A sensitive test of theory is the ability to obtain the correct binary to recoil intensity ratio, which is due to the angular behavior of complex interference cross terms in a partial-wave expansion of the ejected-electron wave function. For s-shell ionization, there is a direct correspondence between this expansion and a multipole expansion of the scattering amplitude. Thus the calculation in-

volves a coherent sum over complex amplitudes, each consisting of a magnitude and a phase, rather than the incoherent sum in integrated scattering cross-section calculations. A recent calculation [3] emphasizes that the binary to recoil intensity ratio depends critically on the phase predictions. The experimental determination of phase information of individual terms is clearly desirable. Traditional coplanar $(e,2e)$ experiments on direct ionization are usually unable to yield complete information about the amplitudes of individual interference cross terms since angular distributions contain a sum over several such terms [4].

In previous exploratory work [5] we have shown how the presence of autoionization enables the isolation of interference effects between the dominant dipole and very weak nondipole processes in the electron-impact ionization of Cd. The experimental technique involves the measurement of coincidence spectra at ejected electron angles 180° apart; small differences in the spectra are due to the sum of interference terms formed from cross products of multipole amplitudes of different parity. These terms are strong functions of ejected-electron energy because of the rapid change of phase across autoionizing resonances. Recently we reported an $(e,2e)$ experiment that enabled the determination of the phase and magnitude of an individual cross term [6]. Below, we report the details of this and other experiments in cadmium that investigate the magnitude and phase of both the monopole and quadrupole amplitudes relative to the dipole amplitude.

II. THEORY

The experiments described here investigate the overall electron-impact ionization process

$$\mathrm{Cd}(5s^{2}\,^{1}S_0)+e_0\rightarrow\mathrm{Cd}^+(5s\,^{2}S_{1/2})+e_{ej}+e_{sc}\;,\qquad(1)$$
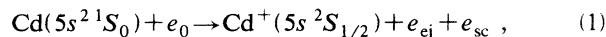
in the region of the $4d^{9}5s^{2}5p$ autoionizing resonances [7]. For comparison with the experiments carried out for $K\approx0.2$ a.u. (for reasons given below), we construct a model based on the plane-wave Born approximation (PWBA). Reference [5] describes a theoretical model that assumes that only autoionization is important for all multipoles; Ref. [6] deals with the case of resonant dipole

---

*Permanent address: Physics Department, Royal Holloway, University of London, Egham, Surrey TW20 0EX, United Kingdom.

and nonresonant monopole ionization. Here we are interested in the possibility of both resonant and nonresonant processes for each multipole.

The final continuum state $|f\rangle$ may be represented as a coherent superposition of total angular momentum basis states

$$|f\rangle = \sum_{LSJM} c_{LSJM} |5sEl\ LSJM\rangle , \qquad (2)$$

where c_{LSJM} are complex coefficients. In the PWBA the summation can be reduced by choosing the quantization axis along the direction of momentum transfer $\mathbf{K}$ (or θ_K), in which case $M=0$ only [8]. Parity-unfavored processes [9], due to the presence of intermediate-coupled Cd autoionizing states [10], may result in the population of triplet continua in addition to the singlet continua allowed by PWBA direct ionization. In terms of LS-coupled continua, the allowed final states are $5sEl^{2S+1}L_J$, where $l=L=J$ and $S=0$ or 1.

The angular distribution of electrons ejected with energy E at angle $\theta=\theta_K-\theta_{ej}$, measured in coincidence with electrons scattered through an angle θ_{sc}, is given by a coherent sum over J but an incoherent sum over S [11,12]:

$$I(\theta_{sc};E,\theta) \sim \sum_{S=0}^{1} \left| \sum_J \left[\frac{(J-S)!}{(J+S)!} \frac{(2J+1)}{2} \right]^{1/2} \right.$$
$$\left. \times b_{JS}(\theta_{sc},E)P_{JS}(\cos\theta) \right|^2 , \qquad (3)$$

where $P_{JS}(\cos\theta)$ is an associated Legendre polynomial for which the radical provides normalization. The complex coefficients $b_{JS}=|b_{JS}|e^{i\delta_{JS}^T}$ describe the ionization process and incorporate the total phase as described below. (We shall always use the symbol θ without a subscript label to mean the ejected-electron direction relative to the momentum transfer direction.) $(e,2e)$ spectra taken at θ and $\theta+\pi$ differ because the parity of the cross terms $P_{JS}P_{J'S}$ is given by $(-1)^{(J+J')}$. We shall denote such pairs of spectra I^+ and I^-, where the positive (negative) sign refers to the binary (recoil) side of the electron beam axis. When $K \ll 1$, the PWBA magnitudes [5,8] are proportional to K^{J-2} for $J>0$, and are independent of K for $J=0$. The present experiments were carried out for $K \approx 0.2$ a.u., which is sufficiently small that the summation in Eq. (3) may be terminated at $J=2$ and the dipole term is much greater than the monopole and quadrupole term. Further simplification is then possible because the $J=0$ even-parity continuum is pure singlet and the Cd $J=2$ autoionizing levels only couple to the singlet $5sEd$ continuum [5]. Thus, for $S=1$, only the $J=1$ term is nonzero in Eq. (3). The *sum* and *difference* spectra are then

$$(I^+ + I^-) \sim 3(|b_{10}|^2\cos^2\theta + \tfrac{1}{2}|b_{11}|^2\sin^2\theta) , \qquad (4)$$

$$(I^+ - I^-) \sim 2\sqrt{3}|b_{10}|$$
$$\times \cos\theta\{ |b_{00}|\cos(\delta_{10}^T - \delta_{00}^T)$$
$$+ \sqrt{5}|b_{20}|\cos(\delta_{10}^T - \delta_{20}^T)P_{20}\} . \qquad (5)$$

In both expressions terms involving the product of two small amplitudes have been dropped. The summed spectrum [Eq. (4)] is a good approximation to the photoelectron angular distribution [13,14], with the parity-favored $(S=0)$ and parity-unfavored $(S=1)$ cross section given by $\sigma_s \propto |b_{1S}|^2$. The difference spectrum reveals the interference cross terms, from which it is possible to obtain magnitude and phase information.

We have carried out extensive pseudorelativistic Hartree-Fock (HFR) calculations [8] to model these equations. Autoionization is included by using Fano-type theories [15,16], in which we assume that all matrix elements are constant over the energy range of interest. The autoionizing levels included are shown in Table I; details of the spectroscopy and excitation mechanisms are given in Ref. [5]. The present HFR calculations differ from our previous model calculation in that PWBA matrix elements have been calculated *ab initio* for autoionizing levels and appropriate continua to enable the construction of all b_{JS}. For the dipole ionization processes both singlet and triplet continua are involved; this is described in Refs. [17,18]. The monopole and quadrupole

TABLE I. Cadmium autoionizing levels (above the 8.99-eV ionization potential) labeled by their largest LS component. Most of the $J=1$ level energies are known experimentally. All other levels are *ab initio* calculated values, adjusted to give a tolerable fit to our data. The $5p^2$ widths are from matrix elements calculated at the $5p6p$ configuration average energy; these differ somewhat from the local values.

			Energy (eV)	Width (eV)
$J=0$	$5p^2$	^3P	0.18	0.0007
		^1S	1.94	0.058
	$5p6p$	^3P	3.69	0.0001
		^1S	4.12	0.0014
	$5p7p$	^3P	4.49	0.0001
		^1S	4.77	0.0005
$J=1$	$4d^95s^25p$	^3P	3.07	0.041
		^1P	3.81	0.140
		^3D	3.94	0.003
	$5p6s$	^3P	2.87	0.054
		^1P	3.19	0.273
	$5p5d$	^3D	3.86	0.003
		^3P	4.03	0.008
		^1P	4.22	0.015
	$5p7s$	^3P	4.34	0.015
		^1P	4.53	0.088
	$5p8s$	^3P	4.82	0.021
		^1P	5.07	0.042
$J=2$	$5p^2$	^3P	0.37	0.019
		^1D	0.88	0.767
	$5p6p$	^3D	3.70	0.009
		^3P	3.98	0.023
		^1D	4.09	0.130
	$5p7p$	^3D	4.54	0.025
		^3P	4.79	0.012
		^1D	4.86	0.098

processes may be calculated from the formalism [15] of several levels E_{Jn} that couple to a single continuum c_J via matrix elements V_{Jn}. For ionization from the ground state g due to a PWBA transition operator $\mathcal{T}$:

$$b_{J0} \propto \cos\Delta_{J0} \left\{ \sum_n \frac{|V_{Jn}|}{E_{Jn}-E} |\langle Jn|\mathcal{T}|g\rangle| \right.$$

$$\left. - |\langle c_J|\mathcal{T}|g\rangle| \right\} e^{i\delta_{J0}^T} \quad (J=0,2) , \qquad (6)$$

where the phase shift due to autoionization is the net shift due to all levels that couple to the same continuum:

$$\tan\Delta_{J0} = \sum_n \frac{\frac{1}{2}\Gamma_{Jn}}{E_{Jn}-E}$$

with level widths $\Gamma_{Jn} = 2\pi|V_{Jn}|^2$. The general form of the total phase is [5]

$$\delta_{JS}^T = \chi_J - \tfrac{1}{2}J\pi + \sigma_J + \delta_{JS} + \Delta_{JS} , \qquad (7)$$

where σ_J is the hydrogenic Coulomb phase, and δ_{JS} is the phase shift due to the unperturbed non-Coulombic ionic potential. The collisional part of the phase is given in the PWBA by $\chi_J = J\pi/2$; notice that it is only because this is the same for both resonant and nonresonant processes that it can be factored out in Eq. (6).

The PWBA matrix elements in Eq. (6) involve single-particle $l_i \rightarrow l_f$ reduced matrix elements [8] $\langle l_f \| j_J(Kr) \| l_i \rangle$, where j_J is a spherical Bessel function of order J. Calculation of the matrix elements for $5s \rightarrow El$ $(l = J = 0,1,2)$, and for the large $J = 1$ autoionizing resonance $4d \rightarrow 5p$, is straightforward. Complications inherent in calculating excitation matrix elements for the doubly excited $5pns,nd$ $J = 1$ autoionizing levels have been discussed elsewhere [19]; the fitted values from this previous work are used here. Excitation matrix elements for the doubly excited $J = 0$ and 2 autoionizing levels were found by multiplying the $5p \rightarrow np$ $(n = 5, 6,$ and 7) calculated value by the $5p^2$ component (0.1774 or about 3%) given by a configuration-interaction (CI) calculation of the mainly $5s^2$ ground state.

From the calculations described above, we reach the following conclusions about the importance of autoionization in the present experiments. The $J = 1$ processes may be modeled extremely accurately. The calculated direct dipole ionization matrix element (for small K) is very small compared to the resonant process via $4d^9 5s^2 5p$; we use the experimental result that direct dipole ionization is negligible [7,18]. The presence of the doubly excited autoionizing states affects the shape of the dipole cross section, but not its integrated intensity; to a good approximation this latter quantity is determined by a single parameter, the $4d \rightarrow 5p$ transition matrix element.

The autoionizing $J = 0$ even-parity states are very narrow and are weakly excited; they have a very local effect on the energy dependence of the monopole amplitude. Thus the overall monopole process is also determined mainly by a single parameter, the $5s \rightarrow Es$ direct ionization matrix element. Hence an experiment that can iso-

late $J = 0,1$ interference (i.e., interference effects between $J = 0$ and $J = 1$) can provide a measure of the relative monopole to dipole amplitude.

The $J = 2$ autoionizing states are wide and have widths comparable to the $J = 1$ resonances as can be seen from Table I. Varying the $J = 2$ resonant to nonresonant relative matrix elements in a calculation of the interference effects shows that autoionization is important, and therefore it is not possible to characterize the $J = 2$ process by a single matrix element. Thus $J = 1,2$ interference effects are due partly to the coherent excitation of overlapping autoionizing levels of differing parity. An analysis of the effects is less straightforward than the $J = 0,1$ case, but is rewarding spectroscopically in that the positions of a number of previously unobserved levels may be tentatively assigned; the $J = 2$ level energies shown in Table I are based on the *ab initio* calculations, adjusted to give a good fit to our experimental data. (Thus these positions differ slightly from those given in earlier reports of these calculations [20].)

An important generalization that emerges from the above model calculations is that when autoionization is present the overall intensity of interference effects is determined by the *magnitude*, whereas the energy dependence depends strongly on the *phase*, of the complex amplitudes [6].

III. EXPERIMENT

The coplanar $(e,2e)$ spectrometer has been described in detail elsewhere [21]. It consists of four main components; an electron gun, a metal-vapor atomic beam oven, a scattered-electron spectrometer, and an ejected-electron spectrometer. The electron gun is recessed in a side arm of the vacuum chamber, which enables the ejected-electron spectrometer to be positioned on both sides of the electron-beam axis. Thus spectra for two ejected-electron angles 180° apart may be taken in a single experimental run at the same value of θ_{sc}.

Previous $(e,2e)$ experiments [5] suffered from low count rates (2 counts/s) and fairly poor energy resolution (150 meV). For the present experiments, the spectrometer has been upgraded by the addition of a resistive anode-type position sensitive detector (PSD) to the ejected-electron channel. This has resulted in improved coincidence count rates (up to 10 c/s) at a greatly improved energy resolution of 40 meV.

Spectrometer control, data acquisition, and analysis are handled by microcomputer. The output strobe from the PSD electronics is used as an interrupt pulse; the position and time information [from a time to amplitude converter (TAC) and analog-to-digital converter (ADC) combination] is then analyzed and recorded by the interrupt-driven software. Thus the interrupt pulse provide a high-quality noncoincident ejected-electron spectrum in addition to the $(e,2e)$ spectrum obtained from the TAC and ADC. The noncoincident spectrum is used for alignment and normalization purposes, as described below. During an experiment, energies and angles are scanned repetitively to minimize the effect of any drift in, for example, the electron-beam intensity.

INVESTIGATION OF COMPLEX IONIZATION AMPLITUDES . . .

IV. RESULTS AND DISCUSSION

Below we describe three experiments in Cd carried out with an incident-electron-beam energy of 150 eV, scattering angles such that $K \approx 0.2$ a.u., and ejected-electron energies $\approx 2.5 \rightarrow 5$ eV. The experiments were carried out at values of θ chosen for the properties of the associated Legendre functions in Eq. (5). Each experiment was designed to examine a different aspect of the interference effects.

A. Magic-angle experiment

For $\theta = \cos^{-1}(\pm\frac{1}{\sqrt{3}}) \approx 54.7(+180)°$—the magic angle —the second-order Legendre polynomial $P_2(\cos\theta)$ (and hence P_{20}) vanishes. This leaves only one term in Eq. (5), between the monopole and dipole amplitudes. Thus the difference spectrum yields the relative amplitude for these processes; the amount of interference is determined by the magnitude ratio, whereas the shape of this spectrum is determined by the relative phase [6].

The experiment was carried out with an electron-beam energy of 150 eV and a scattering angle of $+2°$, corresponding to a momentum transfer of 0.18 a.u. in the spectral region of interest. For this choice of experimental parameters the magic angles correspond to ejected-electron directions of $\pm90°$ with respect to the electron-beam axis. Since our analysis involves the subtraction of two nearly identical spectra, it is vital to normalize and energy align the spectra correctly to one another. Normalization (to better than 2%) and energy alignment (to within 1 meV) of the $(e,2e)$ spectra was achieved for this experiment by using the axial symmetry of the noncoincident ejected spectra. This procedure is shown in Fig. 1, where dissimilar secondary-electron backgrounds from metal surfaces result in a spectral difference curve that is nonzero but perfectly smooth.

The sum and difference $(e,2e)$ spectra are shown in Figs. 2(a) and 2(b). The solid line in Fig. 2(a) is the theoretical dipole cross section folded with a Gaussian of FWHM (full width at half maximum) of 0.04 eV (the instrument function), and satisfactorily fitted to the experimental data to obtain the overall normalization constant (proportional to the dipole matrix element). The calcu-
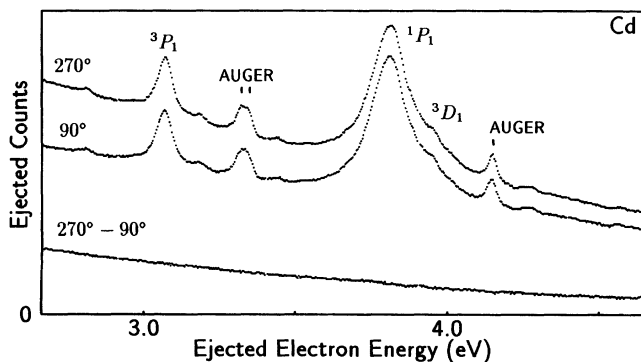
FIG. 1. Experimental Cd ejected-electron spectra, and the difference between them, used for normalizing and aligning magic-angle $(e,2e)$ spectra.
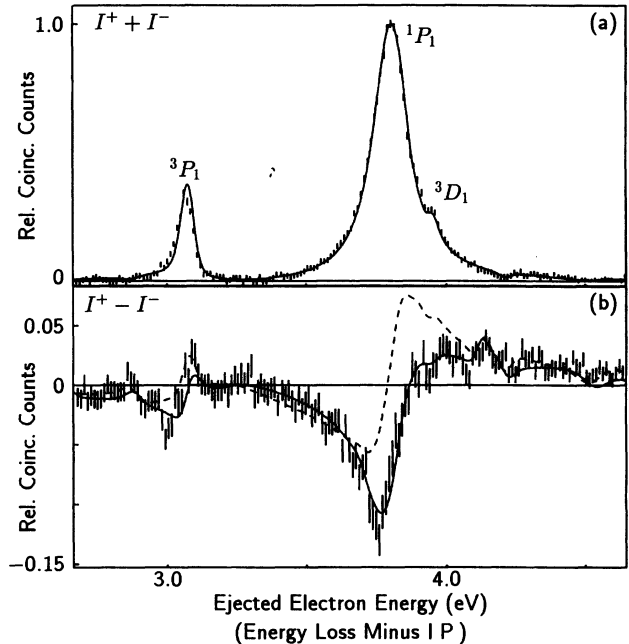
FIG. 2. (a) Experimental magic-angle $(e,2e)$ sum spectrum for Cd. The vertical bars represent the statistical uncertainties. The solid line is the calculated dipole cross section fitted to the data. The three $4d^95s^25p$ autoionizing resonances are labeled. (b) Experimental magic-angle $(e,2e)$ difference spectrum. The solid line is the calculated $J=0,1$ interference fitted to the experimental data. The dashed line is the same calculation but with the PWBA relative phase.

lated PWBA magnitudes and phases do not yield an interference spectrum that agrees with experiment. The solid curve in Fig. 2(b) corresponds to a fitted magnitude ratio

$$\frac{\langle Es\|j_o(Kr)\|5s\rangle}{\langle 5p\|j_1(Kr)\|4d\rangle} = 0.23 \pm 0.02 \ \text{eV}^{-1/2}$$

and a fitted relative phase

$$\chi_{10} = \chi_1 - \chi_0 = (0.20 \pm 0.05)\pi$$

for $K = 0.18$ a.u. and an ejected-electron energy $E \approx 4$ eV. The fitted magnitude ratio is 2.2 times the calculated value, and the fitted phase is 0.3π less than the PWBA relative phase $\pi/2$. The dashed curve in Fig. 2(b) corresponds to the fitted magnitude but the PWBA phase; the difference is most marked in the region of the $^1P_1$ resonance.

In Appendix A we give a simplified analysis of this experiment in the energy region spanned by the nearly Lorentzian $^1P_1$ line shape.

B. Momentum-transfer-axis experiment

For $\theta = 0°$, $180°$ all associated Legendre functions P_{J1} vanish, whereas $|P_{J0}| = |P_J| = 1$, and are maximized. Thus along the momentum transfer axis only parity-

favored ionization processes $(S = 0)$ are observed, for which both $J = 0, 1$, and $J = 1, 2$ interference terms are present in the difference spectrum. Since the solid curve in Fig. 2(b) is a good description of the experimental data, we may use Eq. (5) with the fitted $J = 0, 1$ relative magnitude and phase in order to isolate the $J = 1, 2$ interference.

Spectra were taken for $E_0 = 150$ eV, $\theta_{sc} = +3°$ ($K = 0.22$ a.u.), and $\theta_{ej} = -50°$ and $-230°$, which correspond to the momentum-transfer axis. Alignment and normalization of the spectra was achieved using three Cd Auger peaks [22] in the noncoincident spectra. These have the same intensity for ejected-electron directions 180° apart since they correspond to double ionization, for which the direct process is negligible [23]. Very small differences in energy resolution, thought to be due to stray ac fields, could also be detected and corrected using these narrow peaks. Figure 3(a) and 3(b) show the sum and difference of the noncoincident spectra, after normalization, alignment, and a linear background subtraction to approximate the effects of secondary electron emission. Notice how the Auger peaks, which are prominent in the sum spectrum, have been successfully eliminated in the difference spectrum. This spectrum is discussed further in Appendix B.

The summed $(e, 2e)$ spectrum was satisfactorily fitted to the calculated photoelectron parity-favored cross section, as can be seen in Fig. 4(a). In fact, as discussed elsewhere [14], Eq. (4) omits nondipole terms equal to about 1% of the main $^1P_1$ peak height. To take this into account the data shown in Fig. 4(a) have been background subtracted, which has only 1% effect on the normalization constant, but improves the χ^2 of the fit by a factor of 3.

The difference $(e, 2e)$ spectrum is shown in Fig. 4(b).
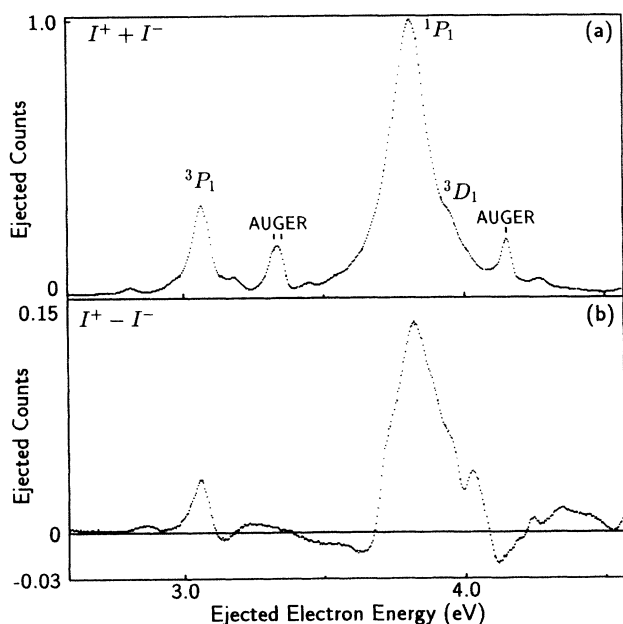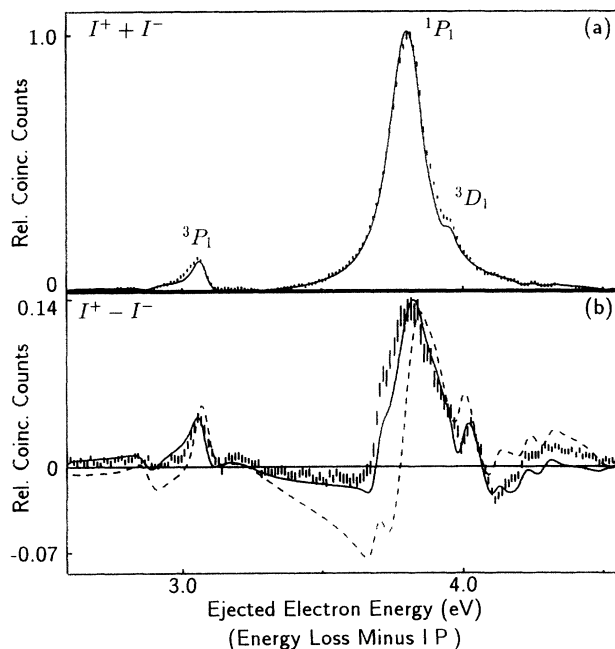
FIG. 4. As Fig. 2, for the momentum-transfer axis experiment. The solid line in (a) is the fitted parity favored cross-section. The solid line in (b) is the calculated $J = 0, 1$ plus fitted $J = 1, 2$ interference. The dashed line is the same calculation but with the PWBA relative phase for $J = 1, 2$.

(This spectrum differs noticeably from our previous exploratory data shown in Fig. 6 of Ref. [5], which suffered from less accurate spectral normalization.) Analysis of this spectrum is complicated since it involves both the spectroscopy of (previously unobserved) $J = 2$ autoionizing levels, and the magnitudes and phases of their ionization amplitudes. However, trial calculations show that the features produced by the autoionizing levels are qualitatively similar over a wide range of ionization amplitudes. We have therefore attempted a spectroscopic analysis before considering the ionization dynamics.

The spectrum shows three striking features that we interpret as being due to $J = 2$ autoionizing levels that overlap, and are coherently excited with, the broad $J = 1$ resonance. These features (and their assignments in Table I) are (a) the sharp rise between 3.67 and 3.72 eV ($5p6p \ ^3D_2$), (b) the sharp minimum at 3.99 eV followed by the pronounced maximum at 4.03 eV ($5p6p \ ^3P_2$), and (c) the broad minimum at 4.11 eV (due to the broad $5p6p \ ^1D_2$). With the exception of feature (a), the $5p6p$ $J = 2$ energies given in Table I are about 0.1 eV higher than the HFR' values, when the latter are referenced to known $5p^2$ levels [24]. We therefore raised the $5p7p$ $J = 2$ levels by the same amount, and obtained quite good agreement with the structure observed above 4.15 eV. Ironically, the only feature detected in the low-resolution exploratory experiments (and assigned to $5p6p \ ^3D_2$ at 3.42 eV [5]) is one of the weakest features in the new high-resolution data. Indeed, in order to explain the above features we have left the 3.42-eV feature unas-

FIG. 3. (a) Sum and (b) difference of ejected-electron spectra for $-50°$ and $-230°$, used for normalizing and aligning $(e, 2e)$ spectra. Notice that the Auger peaks in (a) are absent in (b).

signed in the present work (see also Appendix B).

Following the spectroscopic analysis, the full interference spectrum was calculated using the fitted $J=0,1$ parameters and the *ab initio* PWBA $J=1,2$ magnitude and phase parameters. This calculation did not agree well with the observed data. In view of the large number of autoionizing levels, and hence complex amplitudes (in addition to the direct ionization amplitude), it is difficult to isolate the source of the disagreement. We have therefore tried to find the minimum change to the *ab initio* amplitudes that gives tolerable agreement with the experimental data. The result is shown in Fig. 4(b) as a solid line. This corresponds to (a) leaving the magnitudes for all autoionizing levels as their PWBA values, (b) increasing the direct $5s \rightarrow Ed$ magnitude by a factor of 1.5, and (c) adding $\pi/4$ to the PWBA $\chi_{12}=\chi_1-\chi_2$ relative phase for direct and autoionizing amplitudes; this has the merit of keeping Fano q parameters as real quantities, in keeping with the spirit of the PWBA.

The fitted values are

$$\frac{\langle Ed\|j_2(Kr)\|5s\rangle}{\langle 5p\|j_1(Kr)\|4d\rangle}=0.14\pm0.02 \text{ eV}^{-1/2}$$

and a fitted relative phase

$$\chi_{12}=(-0.25\pm0.05)\pi ,$$

for $K=0.22$ a.u. and an ejected-electron energy of $E\approx4$ eV. The effect of using the above-magnitude ratio, but the PWBA phase, is shown as a dashed line in Fig. 4(b).

The similarities between the $(e,2e)$ and noncoincident different spectra are discussed in Appendix B.

C. $\theta=90°$ experiment

For $\theta=90°$ away from the momentum-transfer axis, Eq. (5) predicts that the difference spectrum vanishes. In fact, within the PWBA, this is true for all $J=0\rightarrow\infty$ and both parity-favored $(S=0)$ and parity-unfavored $(S=1)$ contributions. This follows from the properties of associated Legendre functions and the fact that all cross terms in the difference spectrum require $(J+J')$ odd.

An experiment carried out for $\theta=\pm90°$ is a test of the validity of the PWBA. When the PWBA breaks down and the $\Delta M_J=0$ rule is violated then coherent parity-favored cross terms such as $P_{11}P_{00}\propto\sin\theta$ and $P_{11}P_{20}\propto\sin\theta(\frac{3}{2}\cos^2\theta-\frac{1}{2})$ may occur which contribute to the difference spectrum and do not vanish at $\theta=90°$. (This general result also follows from the argument that the momentum-transfer axis ceases to have special significance when the PWBA is not valid.)

Spectra were taken for $E_0=150$ eV, $\theta_{sc}=-2.75°$ with $\theta_{ej}=-45°$ and $-225°$. These ejected angles lie perpendicular to the momentum-transfer axis. The spectra were aligned and normalized as in the momentum-transfer axis $(\theta=0)$ experiment above; because of the similar ejected-electron angles the noncoincident spectra are almost the same.

The $(e,2e)$ sum and difference spectra are shown in Figs. 5(a) and 5(b). The data have been normalized relative to the $\theta=0$ experiment [Fig. 4(a)] by using the fact
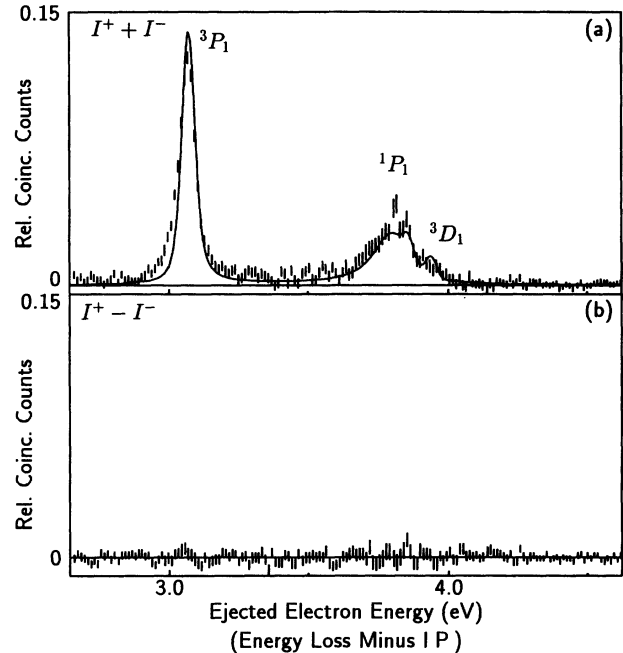
FIG. 5. As Fig. 2, for the $\theta=\pm90°$ experiment. The sum and difference spectra have been normalized to the parity-favored result of Fig. 4(a). The solid line in (a) is the photoelectron cross section (see text).

that the photoelectron angular distribution of the $4d^95s^25p\ {}^3P_1$ resonance is approximately isotropic [13]. The data in Fig. 5(a), although mostly due to the parity-unfavored cross section, contain a small contribution from the parity-favored cross section because of the finite acceptance angle of the scattered detector $(\sim\pm1°)$. This results in spectra averaged over a small range of momentum-transfer directions; the theoretical curve shown in Fig. 5(a) is calculated for an effective ejected-electron direction of 83°.

The finite acceptance angle does not, to first order, affect the difference spectrum, since all cross terms with $(J+J')$ odd change sing as they pass through $\theta=90°$. Thus contributions from $\theta_{sc}\pm\delta\theta_{sc}$ cancel out, to a good approximation, and the difference spectrum shown in Fig. 5(b) is close to the null spectrum expected. We have investigated the possible presence of interference terms, such as those mentioned above, due to the breakdown of the PWBA. The statistical uncertainties place an upper limit on the $4d^95s^25p$ excitation amplitude ratio of the dipole $|\Delta M_J|=1$ to $|\Delta M_J|=0$ processes of about 3%. This corresponds to an upper limit, on this aspect of the breakdown of the PWBA, that may be expressed as a cross-section ratio $\sigma_{11}/\sigma_{10}\leq10^{-3}$.

V. CONCLUSIONS

A number of high-resolution $(e,2e)$ experiments in Cd, and calculations to aid in their interpretation, have been carried out for intermediate incident electron energy and small momentum transfer $K\approx0.2$ a.u. Interference effects have been observed in $(e,2e)$ spectra due to the

coherent excitation of autoionizing resonances and continua of differing total angular momentum and parity. We have obtained relative magnitudes and phases for $J=0$ and 1 ionization amplitudes from an experiment that isolates interferences between direct monopole ionization and dipole autoionization. For $J=2$ we find that both autoionization and direct ionization are important. We have obtained tentative values for the relative magnitude and phase of direct quadrupole ionization and dipole autoionization.

We find that the PWBA predicts relative excitation magnitudes that are incorrect by a factor of 2. The PWBA relative phases differ from the experimentally obtained values by approximately $\pm\pi/4$ in the two cases. The phase (but not the magnitude) findings are in agreement with a recent calculation [3] of carbon inner-shell ionization that compared the PWBA and Coulomb Born approximation (CBA). This calculation found that there was little difference between multipole magnitudes, but considerable difference in their relative phases, in the two approximations. The CBA yielded relative $J=0,1$ and $J=1,2$ phases that differed from the PWBA results by amounts similar in size to, and with the same sign as, those in our experiments.

Experiments are currently under way to repeat the measurements presented here but at larger scattering angles. For an incident electron energy of 150 eV, the range $0.2 < K < 1$ corresponds to $\theta_{sc} \leq 20°$. It is to be hoped that the present paper, and these experiments in progress, will stimulate more sophisticated calculations, such as distorted-wave Born amplitudes, for Cd ionization by electron impact.

ACKNOWLEDGMENTS

APPENDIX A

The $J=0,1$ difference spectrum, observed in the magic-angle experiment, may be approximated, in the region of the strong $^1P_1$ resonance, by direct $J=0$ ionization interfering with a single broad autoionizing $J=1$ level at energy E_R which couples only to the singlet continuum with a discrete-continuum matrix element V. The autoionization is characterized by a phase [15]

$$\cot\Delta_{10} = -\varepsilon = -\frac{(E-E_R)}{\Gamma/2} , \qquad (A1)$$

leading to a Lorentzian line shape $\sin^2\Delta_{10}$ with full width at half maximum $\Gamma = 2\pi V^2 = 0.14$ eV. Equations (4) and (5) may then be simplified, for the magic-angle experiment, to yield the ratio of the difference and sum intensities in terms of the reduced energy ε and constant nonresonant monopole and resonant dipole amplitudes a_0
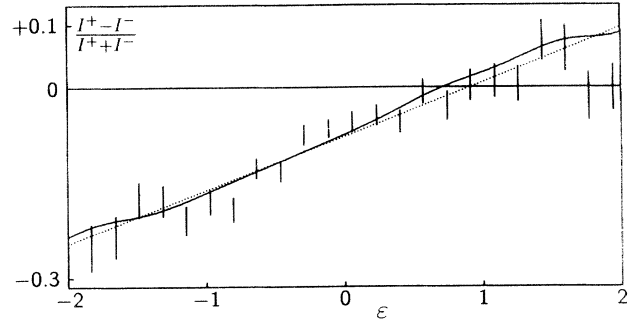
FIG. 6. The data of Fig. 2 presented as the ratio of the difference and sum spectra in the $^1P_1$ region. The solid line is a calculation including all autoionizing levels. The dotted line is a straight-line fit in the spirit of Eq. (A2).

and A_1, respectively:

$$\frac{I^+-I^-}{I^++I^-} = 2\pi V\frac{|a_0|}{|A_1|}\cos\delta_{10}^T[\varepsilon+\tan\delta_{10}^T] , \qquad (A2)$$

which is a straight line whose intercept on the ε axis gives the relative phase and whose slope then gives the relative magnitude. The experimental data are presented in this form in Fig. 6. The solid curve is the full theory, which includes all resonances, fitted to the data (i.e., the ratio of the theoretical curves in Figs. 2). The dotted line is the best straight-line fit, which, using Eq. (A2), corresponds to $\chi_{10}=0.17\pi$ and a relative magnitude within 10% of the fitted value. It is remarkable that the simple analysis is applicable within the range $\varepsilon=\pm2$, given the complexity of the dipole spectrum.

APPENDIX B

The noncoincident difference spectrum and the $(e,2e)$ difference spectrum of the momentum-transfer axis experiment [Figs. 3(b) and 4(b)] are remarkably similar, both qualitatively and quantitatively. To bring out the similarities, Fig. 7 shows these two plots superimposed. That the similarities are not due to an instrumental effect can be deduced from the $\theta=\pm90°$ experiment whose noncoincident difference spectrum is virtually identical to Fig. 3(b), but whose $(e,2e)$ difference spectrum is the null spectrum of Fig. 5(b).

The noncoincidence spectra correspond to $(e,2e)$ spectra integrated over all scattering angles. Thus there are contributions from scattering angles greater than 3° for which multipoles higher than those included in Eq. (5) are significant for the ionization process. If the dipole term is still the largest, additions to the interference spectrum will mainly be due to cross terms of $J=1$ with the even-parity continua $J=4,6,\ldots$. Since there are no even-parity Cd autoionizing levels with $J>2$ in this part of the spectrum, each extra interference term will be similar to $J=0,1$ interference to within an overall phase. The noncoincident spectrum, for any θ_{ej}, is then given by an expression very similar to Eq. (5), integrated over scatter-
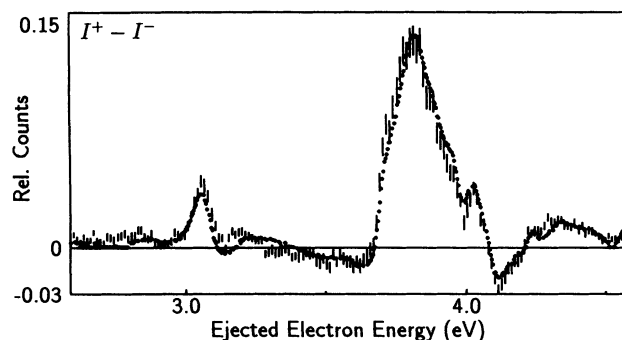
FIG. 7. A quantitative comparison of (●) noncoincident [Fig. 3(b)] and (|) coincident [Fig. 4(b)] difference spectra. Both spectra are normalized with respect to the appropriate sum spectrum.

ing angle. In other words, the form of the noncoincident difference spectrum will be given by Eq. (5) with averaged magnitudes and phases for each of the two terms. Thus some qualitative similarities between noncoincident and coincident difference spectra are to be expected. That these averaged values for $\theta_{ej}=50°$ and $230°$ are virtually identical to those for the $\theta_{sc}=3°$ $(e,2e)$ difference spectrum along the momentum-transfer axis is presumably serendipitous.

The minimum at 4.15 eV in the $(e,2e)$ difference spectrum is due to $J=1,2$ interference. We have carried out trial calculations that show that the intensity ratio of the maximum at 3.8 eV to this minimum is very dependent on the relative phase of the $J=1,2$ amplitudes. Since this ratio is the same in the non-coincidence difference spectrum, we may deduce that the $J=1,2$ relative phase is independent of scattering angle over the range of angles important for the integrated spectrum; i.e., this phase disagrees with the PWBA results by $\pi/4$, and this extra phase is insensitive to scattering angle.

There is only one noticeable difference between the spectra in Fig. 7: the position of the shallow maximum above $4d^9 5s^2 5p\ ^3P_1$ differs by 0.05 eV. Our calculations show that this can be reproduced by introducing a nonzero direct dipole ionization amplitude; indeed, the PWBA calculations indicate that this is to be expected as θ_{sc} increases.

One interesting consequence of the similarities in the noncoincident and $(e,2e)$ spectra is the possibility of examining the former in more detail; i.e., at an energy resolution where the coincidence count rate is too low to be viable. [For the $\theta=0$ experiment with the present resolution, the noncoincident count rate is 100 times higher than the $(e,2e)$ count rate.] Here we note that the excellent statistics of the noncoincident spectra reveal that the point of inflection at 3.42 eV is a smooth feature rather than the sharp one expected from a narrow autoionizing level.

[1] C. J. Joachain and B. Piraux, Comments At. Mol. Phys. 17, 261 (1986).

[2] A. Lahmam-Bennani, J. Phys. B 24, 2401 (1991).

[3] J. Botero and J. H. Macek, Phys. Rev. A 45, 154 (1992).

[4] P. L. Altick and T. Rösel, J. Phys. B 21, 2635 (1988).

[5] N. L. S. Martin and D. B. Thompson, Phys. Rev. A 43, 2281 (1991).

[6] N. L. S. Martin, D. B. Thompson, R. P. Bauman, and M. Wilson, Phys. Rev. Lett. 72, 2163 (1994).

[7] G. V. Marr and J. M. Austin, Proc. R. Soc. London, Ser. A 310, 137 (1969).

[8] R. D. Cowan, The Theory of Atomic Structure and Spectra (University of California Press, Berkeley, 1981).

[9] U. Fano and D. Dill, Phys. Rev. A 6, 185 (1972); D. Dill, ibid. 7, 1976 (1973).

[10] M. Wilson, J. Phys. B 1, 736 (1968).

[11] V. V. Balashov, S. S. Lipovetsky, and V. S. Senashenko, Zh. Eksp. Teor. Fiz. 63, 1622 (1972) [Sov. Phys. JETP 36, 858 (1973)].

[12] C. E. Theodosiou, Phys. Rev. A 16, 2232 (1977).

[13] J. Jimenez-Mier, C. D. Caldwell, and M. O. Krause, Phys. Rev. A 39, 95 (1989).

[14] N. L. S. Martin, D. B. Thompson, R. P. Bauman, M. Wilson, J. Jiménez-Mier, C. D. Caldwell and M. O. Krause,

J. Phys. B 27, 3945 (1994).

[15] U. Fano, Phys. Rev. 124, 1866 (1961).

[16] E. B. Saloman, J. W. Cooper and D. E. Kelleher, Phys. Rev. Lett. 55, 193 (1985); D. E. Kelleher, in Proceedings of the Fifth International Conference on Spectral Line Shapes, edited by B. Wende (De Gruyter, Berlin, 1981), p. 281, and private communication.

[17] N. L. S. Martin, Nucl. Instrum. Methods B 40/41, 228 (1989).

[18] N. L. S. Martin, J. Phys. B 23, 2223 (1990).

[19] N. L. S. Martin and M. Wilson, J. Phys. B Lett. 25, L463 (1992).

[20] N. L. S. Martin, D. B. Thompson, R. P. Bauman, and M. Wilson, J. Phys. IV (France) Colloq. 3, C6-69 (1993).

[21] N. L. S. Martin and D. B. Thompson, J. Phys. B 24, 683 (1991).

[22] V. Pejčev, K. J. Ross, D. Rassi, and T. W. Ottley, J. Phys. B 10, 459 (1977).

[23] W. Melhorn, in Atomic Inner-Shell Physics, edited by B. Crasemann (Plenum, New York, 1985), p. 119.

[24] C. E. Moore, Atomic Energy Levels, Natl. Bur. Stand. (U.S.) Circ. No. 467 (U.S. GPO, Washington, DC, 1958), Vol. III.